Journal of Geochemical Exploration 184 (2018) 1–10

Contents lists available at ScienceDirect

Journal of Geochemical Exploration

journal homepage: www.elsevier.com/locate/gexplo

Heavy mineral analysis by ICP-AES a tool to aid sediment provenancing

I. Mounteney*, A.K. Burton, A.R. Farrant, M.J. Watts, S.J. Kemp, J.M. Cook

British Geological Survey, Nottingham NG12 5GG, UK

ARTICLE INFO

Keywords:
Heavy minerals
ICP-AES
Provenance studies
United Arab Emirates
Geochemistry

ABSTRACT

Correlation and provenancing of sediments/sedimentary rocks can be achieved by several techniques; a common approach is through the identification and quantification of heavy minerals using a petrological microscope. This can be time consuming, the analysis of heavy minerals by inductively coupled plasma atomic emission spectroscopy offers a faster alternative, by determining key elements associated with specific heavy minerals. Here we outline a method for determining heavy mineral species though ICP-AES using high temperature fusion with a lithium metaborate flux to ensure complete dissolution of resistate minerals. The method was tested in a provenance study of desert sands from the United Arab Emirates. The results are compared with those derived from traditional optical microscopy. These show good agreement for minerals with specific geochemical signatures, whilst the overall geochemistry of the heavy mineral concentrate was diagnostic of potential sediment sources. This geochemical approach is capable of processing large numbers of samples rapidly and is advocated as a screening technique. A combination of geochemical and mineralogical data produced by these techniques provides a powerful diagnostic tool for studies of heavy mineral signatures in sediments frequently used in mineral reconnaissance, paleogeographic reconstruction and reservoir characterisation in the petroleum industry.

1. Introduction

Understanding the origin or provenance of sediments/sedimentary rocks is important in the reconstruction of sediment pathways and paleogeography (Garzanti et al., 2007 and Weltje and Eynatten, 2004), as a tool for mineral reconnaissance (Morton and Berge, 1995), or oil and gas reservoir characterisation (Averill, 2001). Heavy mineral provenancing is traditionally carried out through the identification and quantification of heavy mineral concentrates using a petrological microscope (Morton and Hallsworth, 1993). The main advantage of analysing the heavy mineral fraction is to reduce the dilution from minerals such as quartz, feldspars, carbonate and clays that can typically constitute up to 99% of the sediment and are not generally provenance specific (Morton and Hallsworth, 1999).

Optical microscopy provides information on grain morphology, physico-chemical alteration and the accurate identification of individual heavy mineral species. Such detailed assessment of mineral concentrates can aid in assessing whether the heavy mineral component of a sediment has been altered through selective dissolution, diagenesis or preferential sorting during transportation (Andò et al., 2012). The disadvantages, however, include the difficulty in identifying opaque minerals, the potential for human error and the time associated in undertaking a study with numerous samples. An experienced analyst can analyse an average of three samples per day, involving the identification of 300–500 non-opaque heavy minerals per sample (Morton and Hallsworth, 1993). Minerals excluded from the count include opaque minerals (e.g. magnetite, ilmenite), minerals that are potentially unrepresentative (carbonates, authigenic minerals) or minerals whose specific density is affected by inclusions of another mineral of greater density (magnetite, ilmenite, etc.) than that of the host mineral (Hounslow and Morton, 2004).

Optical identification of the heavy minerals is typically achieved using a standard ribbon counting method (Galehouse, 1971). Provenance is determined by focusing on specific pairs of minerals with similar shape, density and resistance to alteration to create a mineral index, e.g. rutile zircon index [RZi] or chrome-spinel zircon [CZi]. One or more mineral indices are chosen to differentiate sediment sources (Morton and Hallsworth, 1993 and Garzanti et al., 2013). Heavy minerals can be further divided into those that are inherently resistant to weathering, dissolution and transportation (e.g. zircon, monazite, tourmaline and rutile) and those that are less resistant (typically olivine, pyroxene and amphibole) (Garzanti et al., 2013).

Some of the earliest provenance based studies employed mineral-chemical associations using atomic absorption spectrometry (AAS) (Luepke, 1980). For this technique, large volumes of sediment were required to obtain sufficient heavy mineral concentrate for analysis and

* Corresponding author.
E-mail address: Iaian1@bgs.ac.uk (I. Mounteney).

http://dx.doi.org/10.1016/j.gexplo.2017.10.007
Received 23 March 2017; Received in revised form 21 September 2017; Accepted 4 October 2017
Available online 07 October 2017

the data interpretation was limited by the relatively poor detection limits of the AAS technique. Recent provenance studies based on heavy minerals still rely on optical microscopy supported by whole-rock chemical data obtained by inductively coupled plasma-atomic emission spectroscopy (ICP-AES), inductively coupled plasma-mass spectroscopy (ICP-MS), qualitative evaluation of materials by scanning electron microscope (QEM*SEM) or X-ray diffraction (XRD) on bulk samples (Pearce et al., 2010 and Pe-Piper et al., 2016). Raman spectrometry is also used to aid in the identification of single heavy minerals (Worobiec et al., 2007). Current ICP technology, combined with appropriate dissolution procedure, is capable of producing geochemical data for a large number of heavy mineral separates rapidly due to dual-view plasma optics and better optical resolution. Combined with a better understanding of provenance indicators, the associated geochemistry can be employed as a prescreening technique or as a complimentary method which can be used concurrently with optical microscopy.

A wide selection of sample dissolution procedures have been employed for geochemical analysis by ICP-AES (Miles and Cook, 2007). These usually involve decomposition with mineral acids either with or without hydrofluoric acid; or fusion with a flux such as lithium metaborate or alkali metal carbonates, oxides or hydroxides. In general, fusion techniques are more effective at dissolving resistant minerals, such as zircons, than acid digestions. Poor recoveries of Zr from granites, rhyolites, andesites and low Cr recoveries from harzburgites are typically evident of incomplete digestions (Lapworth et al., 2012).

Analysis of heavy mineral concentrates by ICP-AES following an appropriate digestion offers a novel approach to provenance studies which is inherently faster than traditional microscopy. A throughput of at least 30 samples per day can be achieved by ICP-AES, including sample fusion and subsequent dissolution, representing a ten-fold increase in productivity compared to analysis by optical microscopy. Fandrich et al. (2007), also acknowledged the time consuming nature of ore characterisation using optical microscopy compared to QEM*SEM analysis.

Where the elemental composition of a heavy mineral concentrate is not diagnostic of a particular mineral phase, its geochemical signature can, in certain cases, still be diagnostic of a specific geological terrain. For example, a mafic or ophiolitic terrain would tend to be enriched in Cr, Fe, Ni, Ti, and Mg (Wallace et al., 2015) whilst a granitic source would be dominated by Ca, P, Ti and Zr (Arslan and Aslan, 2006) and a high grade metamorphic terrain would be represented by increased Al, Ca, Fe, and Mg (Sukhorukov, 2007). However, reconstructing sedimentary pathways are rarely this simple; geological terrains are often complex, constructed of multiple lithologies, and/or sedimentary basins could be infilled from several sources, over a period of time. In this instance, the geochemistry may not necessarily be diagnostic of a specific geological terrain but may still yield valuable data.

In this paper we demonstrate the validity of a geochemical approach to heavy mineral provenance studies, by comparing the interpretation of geochemical data with results from the traditional optical microscopy. Data was acquired through a provenance study of the Rub' al Khali desert sands of the United Arab Emirates (UAE) (Fig. 1).

2. Materials

2.1. Study location

The Rub' al Khali (Arabic for ‘empty quarter’) desert of the UAE is one of the largest free-moving bodies of sand on Earth (Kumar and Abdullah, 2011 and Glennie and Singhvi, 2002). It was formed in a Neogene elongate basin at the southern end of the Arabian Peninsula and is characterised by large sand dunes up to 250 m in height (Kumar and Abdullah, 2011 and Glennie and Singhvi, 2002). This enormous body of sand was previously interpreted as being derived from several sources including the Arabian Shield, Hajar Mountains and Zagros Mountains (Garzanti et al., 2013, Garzanti et al., 2003, Crouvi et al., 2010 and Evans and Carter, 2002). Geological mapping of the UAE (Farrant et al., 2012) indicate four main sediment facies along the northern upwind margin of the Rub' al Khali desert varying in age from Miocene to Quaternary. These include: 1. Miocene age fluvial sandstones exposed along the Arabian Gulf coast derived from the Arabian shield; 2. Quaternary palaeodune sandstones of the Ghayathi Formation derived from sediments washed into the Arabian Gulf; 3. Quaternary fluvial fanglomerates and sandstones emanating out from the Hajar Mountains (Hili Formation); and 4. Quaternary to recent aeolian dune sediments representing a variable mix of sediment sources, blown inland by the northwesterly Shamal winds (Kumar and Abdullah, 2011 and Edgell, 2006) (Fig. 1). The detrital heavy-mineral assemblages for the studied samples are dominated by ferromagnesian minerals (average 36%); including calcic amphibole (25.8%), clinopyroxene (6.8%) and orthopyroxene (3.4%). The other major constituents are epidote (35.7%), garnet (12.6%). The remaining mineral phases include: apatite (1.1%), Cr-spinel (3.0%), rutile (1.2%), staurolite (0.5%), titanite (1.5%), tourmaline (3.1%) and zircon (4.3%). The remaining 1% of the averaged heavy mineral component includes trace quantities of the minerals andalusite, brookite, glaucophane, kyanite, monazite, sillimanite and blue-green spinel.

3. Methods

3.1. Reagents and standards

Samples and reference materials (RMs) were fused using lithium metaborate ($LiBO_2$) [Sigma-Aldrich: 99.9% trace metals basis] and sodium peroxide (Na_2O_2) [Acros organics 96%]. All concentrated acids and hydrogen peroxide (H_2O_2) used in the digestions were Romil-SpA™ super purity reagents. Deionised water (Milli-Q™) with a resistivity of 18.2 MΩ cm at 25 °C was used for all dissolutions and dilutions.

A certified RM NIM-D (dunite) from the National Institute for Metallurgy, Republic of South Africa and the three in-house AHMCs were included in each batch of fusions. Aqueous ICP-AES calibration standards in 5% HNO_3 were prepared on the day of analysis from ROMIL PrimAg® single element standards. Three independent quality control (QC) standards in 5% HNO_3 prepared from Fisher Scientific single element ICP solutions were incorporated in each analytical run. Independent analytical QC solutions were prepared from a Perkin Elmer Pure multi-element standard (As, Ba, K, La, Mg, Mn, Ni, Sr and Zn) and SPEX CertiPrep® standards 1 (As, Ba, K, La, Mg, Mn, Ni, Sr and Zn) and 4 (Mo, P, S, Si, Ti and Zr).

3.2. Artificial heavy mineral concentrates

Three artificial heavy mineral concentrates (AHMCs) were created to provide a standard concentrate with a known mineral and chemical composition for the development of a robust fusion method and for use as quality control materials during routine analysis. They were created by mixing pure minerals in varying proportions (Table 1) to reflect the average assemblages of naturally occurring heavy mineral concentrates (HMCs), the chosen minerals are representative of the natural concentrates associated with those sampled in the UAE. The major and trace element composition of these AHMCs were determined by wavelength dispersive X-ray fluorescence spectrometry (XRFS). Fused beads (pre-ignited and prepared in a lithium tetraborate/metaborate flux) were analysed on a PANalytical Axios mAX WD-XRF spectrometer using Omnian interpretative software.

3.3. AHMC sample dissolution

Three different methods for the dissolution of AHMCs were assessed:

- HF-mixed acid (HNO_3, HF and $HClO_4$ acids plus H_2O_2) digestion in a

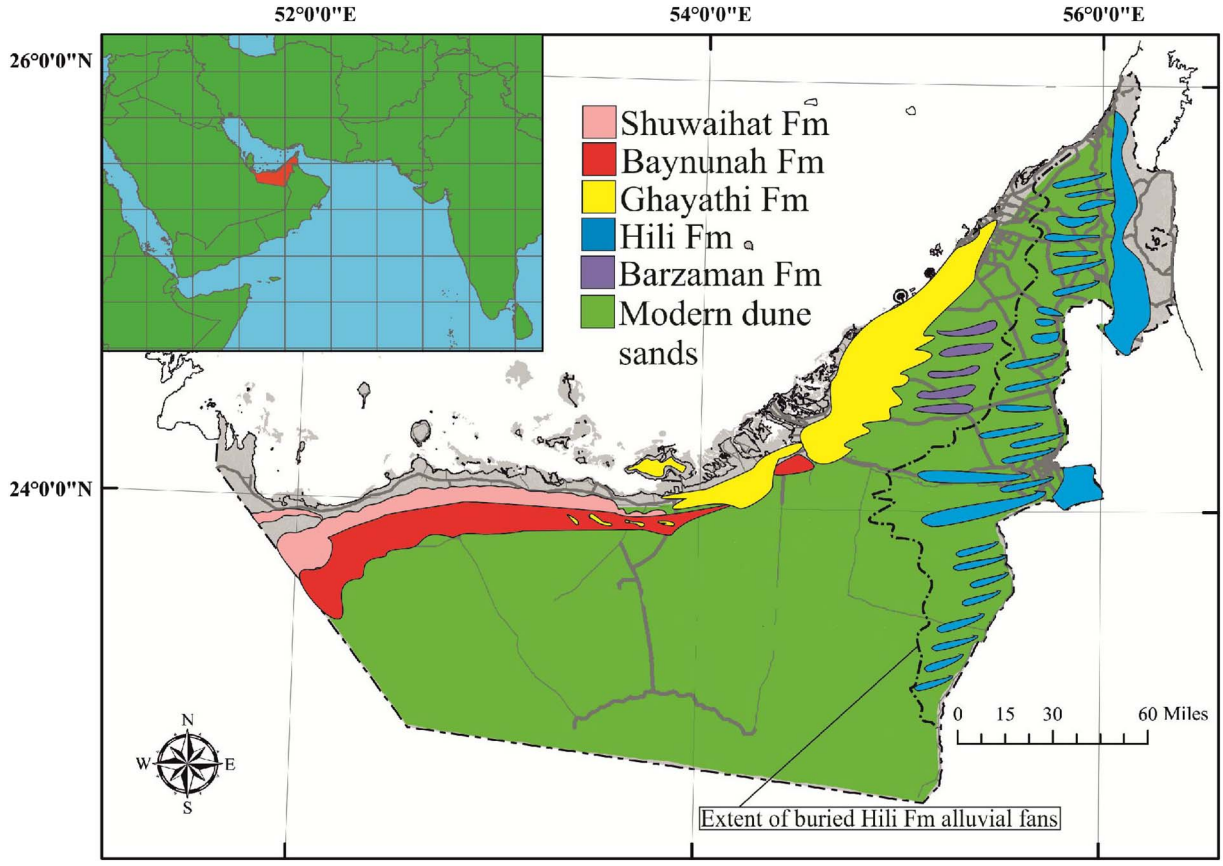

Fig. 1. Location of the United Arab Emirates and simplified geological map, Miocene sediments include the Shuwaihat and Baynunah formations. Created using ArcGIS, [version 10.1], (http://desktop.arcgis.com/en/arcmap).

programmable hot-block (Watts et al., 2008 and Joy et al., 2015).

- A ramped fusion with Na_2O_2 at 550 °C followed by dissolution in HCl and HF acids (Watts and Chenery, 2010).
- Flash-fusion at 1050 °C with $LiBO_2$, followed by dissolution in a mixture of HNO_3 and HF acids.

The relative effectiveness of these sample dissolution methods is summarised in Table 2. This shows the percentage recovery for a range of key major and minor elements compared to the total concentration data obtained by XRFS. Each fusion or digestion was performed in triplicate. The very low recoveries for some elements, especially Cr and Zr (1 to 6%), by the HF-hot block method indicate an almost incomplete dissolution of the resistate minerals zircon and chrome-spinel. Fe concentration was greater than the upper calibration limit for the defined method, but due to the incomplete digestion of Cr and Zr phases, repeat at further dilution was not performed. Mean recoveries for Cr and Zr

Table 1
Composition of the three Artificial Heavy Mineral Concentrates (AHMCs); formulas included are for reference and do not reflect the composition of the minerals used.

Mineral	Formula	AHMC1 (%)	AHMC2 (%)	AHMC3 (%)
Apatite	$Ca_5(PO_4)3F$	0.6	13.5	19.9
Augite (Clinopyroxene)	$Ca_{0.9}Na_{0.1}Mg_{0.9}Fe^{2+}_{0.2}Al_{0.4}\ Ti_{0.1}Si_{1.9}O_6$	19.8	0	0.6
Chrome spinel	$Fe^{2+}\ Cr_2O_4$	5	0.9	10.4
Dolomite	$CaMg(CO_3)_2$	0.6	13.4	0.5
Elbaite (Tourmaline)	$NaLi_{2.5}Al_{6.5}(BO_3)_3Si_6O_{18}\ (OH)_4$	10.7	7	10.4
Enstatite (Orthopyroxene)	$Mg_2Si_2O_6$	19.8	1	10.4
Epidote	Ca_2Fe_3 + 2.25Al $0.75(SiO_4)_3(OH)$	2	0.1	1.05
Haematite	Fe_2O_3	0.6	0.9	0.5
Hornblende	$(Ca,Na)_{2-3}(Mg,Fe,Al)_5$	19.8	0	0.5
Ilmenite	$FeTiO_3$	5	7	6
Monazite	$(Ce,La)PO_4$	0.7	13.5	6
Pyrope (Garnet)	$Mg_3Al_2(SiO_4)_3$	5.2	13.5	6.1
Rutile	TiO_2	5	1	6
Titanite	$CaTiSiO_5$	5	13.5	10.5
Staurolite	$Fe^{2+}_{1.4}Li_{0.1}Mg_{0.1}Al_{8.6}Si_{3.9}$	0	7	0.6
Zircon	$ZrSiO_4$	0.7	7	10.4
Zoisite	$Ca_2Al_3Si_3O_{12}(OH)$	0.8	1	0.5

Table 2
Percent recovery for AHMC standards determined by ICP-AES digested by three different methods in triplicate compared to XRFS data (N/A = not applicable).

Sample digestion	AHMC	Si	Ti	Al	Fe	Mn	Mg	Ca	Cr	P	Zr
HF hot	AHMC1	N/A	49	60	149	98	67	99	1	35	6
block	AHMC2	N/A	71	38	143	108	67	101	6	27	1
digest	AHMC3	N/A	46	49	131	81	36	105	2	36	1
Na_2O_2	AHMC1	101	96	100	96	94	92	93	67	206	105
fusion	AHMC2	98	91	98	94	102	87	85	87	94	81
	AHMC3	96	89	97	89	86	87	85	69	92	73
$LiBO_2$	AHMC1	98	100	101	102	95	97	98	95	100	82
fusion	AHMC2	102	98	103	104	105	95	94	109	99	105
	AHMC3	110	101	107	103	96	101	98	98	96	103

using a Na_2O_2 fusion were 74% and 86%, respectively. The efficiency of this fusion decreased with increasing zircon content (AHMC1 = 105%, AHMC2 = 81% and AHMC3 = 73% zircon). An anomalous 206% recovery of P for AHMC1 is due to a single high P result; due to the overall poor Cr and Zr values, this was disregarded.

Fusion with $LiBO_2$ provided the most complete digestion and was identified as the most appropriate method for the dissolution of heavy minerals. During the main study, 37 AHMCs were analysed (see supplementary data for full AHMC data) during the analysis of the UAE heavy mineral concentrates and performance data is illustrated in Fig. 2.

Correlations between the percentage of mineral(s) within the AHMC's and the ICP-AES data can be used to construct a representative calibration curve. Fig. 3 shows four calibration curves, three of these calibrations display good correlations with corresponding R^2 values: Cr, $R^2 = 0.99$, P, $R^2 = 0.96$ and Zr, $R^2 = 0.99$, however, Ti has a poor calibration correlation ($R^2 = 0.22$). The AHMC's have the following percentages of major Ti bearing minerals (ilmenite, rutile and titanite): AHMC1 15%, AHMC2 21.4% and AHMC3 22.6%, however, AHMC1 has 20% augite (clinopyroxene), which, with a presumed Ti content of 2.03% would still greatly influence the Ti content of AHMC1.

3.4. Sample preparation

A total of 118 samples were selected for analysis, constituting of the four aforementioned sediments (1. Miocene age fluvial sandstones, 2. Ghayathi Formation, 3. Hili Formation and 4. Dune sands of Quaternary to recent age). Subsamples ranging from 100 to 200 g were separated, disaggregated with a pestle and mortar if required, and dispersed in deionised water using a reciprocal shaker overnight. The samples were then sieved to produce a 63–125 μm (fine sand) fraction and then dried overnight before separation of the heavy minerals using a lithium heteropolytungstate heavy liquid at a density of 2.85 g/cm^3 (LST-Fastfloat™). The average heavy mineral yield for the 63 to 125 μm fraction was 4%. A representative subsample was mounted on a glass side using Canada Balsm. An average of 600 transparent grains was counted per sample using a standard ribbon counting method (Galehouse, 1971).

3.5. Analytical method for ICP-AES determinations

A representative sub-sample of each HMC from the UAE was retained for optical microscopy and the remaining sample was micronised to reduce the particle size to < 20 μm. A 0.1 g portion of the milled concentrate was fused with 0.9 g $LiBO_2$ flux in a platinum crucible and flash-fused at 1050 °C for 15 min in batches of 30, which included one fusion blank, one duplicate, two AHMCs and a CRM (NIM-D). When cool, the crucibles were placed into vessels containing 50 mL deionised water, 5 mL conc. HNO_3 and 1 mL conc. HF, capped and placed on a reciprocal shaker overnight. After 18 h, a further 44 mL deionised water was added to the vessels prior to analysis (see supplementary data for a full suite of elements for all 118 samples from the UAE).

To compensate for any potential enhancement of the analytical signal due to the increased ionisation potential of lithium ions in the plasma, calibration standards, blanks and QC solutions were matrix-matched using 10% 0.18 mol L^{-1} $LiBO_2$. Samples were diluted by a factor of 10, therefore the analysed molarity for both samples and standards was 0.018 mol L^{-1} $LiBO_2$. Analyte wavelengths were chosen to minimise any spectral interferences. Major elements were determined using a Perkin Elmer 7300 DV instrument in radial view mode to limit saturation of the segmented-array charge-coupled device detectors, whilst trace elements were measured in axial mode for higher sensitivity and better detection limits. Instrumental parameters specific to the analysis of HMCs by ICP-AES are given in Table 3.

4. Results

In order to compare the performance characteristics of elements with concentration ranges that varied over several orders of magnitude, the data were first normalised by setting the minimum and maximum concentrations of each element to 0 and 1 (Kumar-Jain and Bhandare, 2011). Mineralogical data were normalised using the same method to provide comparable data.

A direct relationship between the mineralogical and geochemical

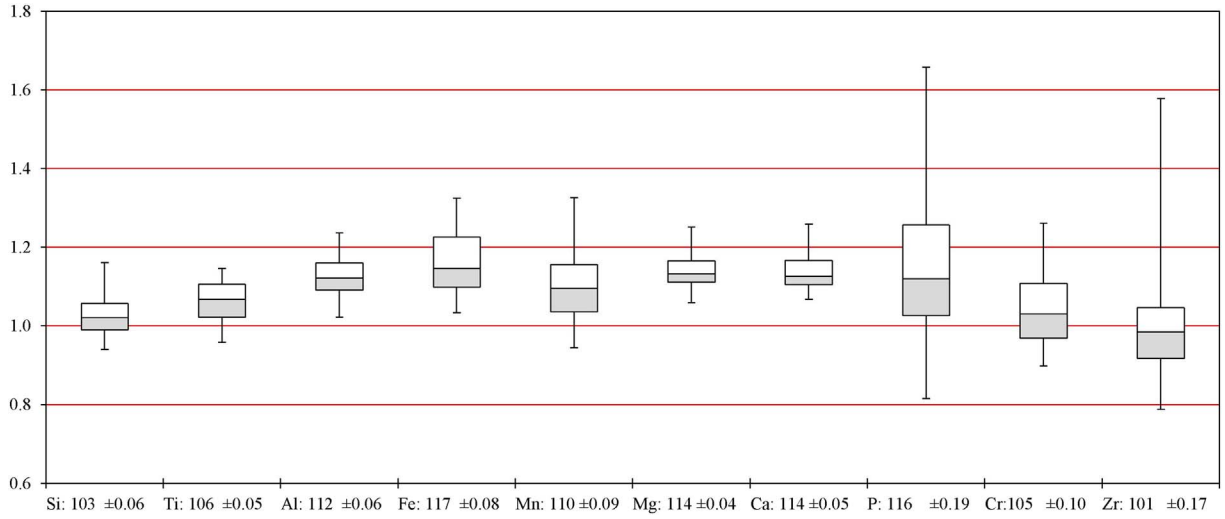

Fig. 2. Box and whisker plot for 37 AHMC QCs.

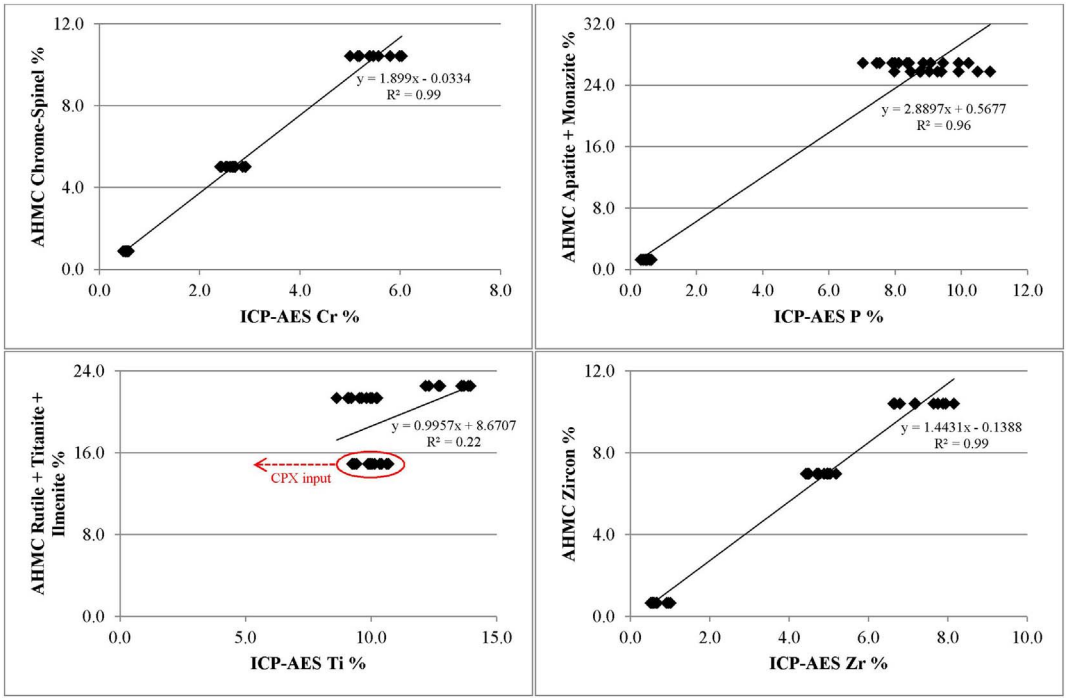

Fig. 3. Calibration plots for AHMC content and ICP-AES geochemistry: Cr, P, Ti and Zr (%).

Table 3
Instrument parameters for analysing HMCs by ICP-AES.

Instrument	Perkin Elmer Optima 7300 dual view ICP-AES
Detector	Segmented-array charge-coupled device
RF generator	Solid state
Plasma power (watts)	1400 watts
Argon flow (carrier gas flow)	1.4 L min^{-1}
Sample uptake rate	1.0 mL min^{-1}
Nebuliser	Meinhard C type
Spray chamber	Cyclonic
Replicates per sample	3
Sample uptake delay	60 s
Wash time	60 s
Nebuliser flow rate	0.65 L min^{-1}
Points per peak	3
Background correction	2 point
Wash solution	5% HNO_3
Software	WinLab 5.5
Major elements	Al, Ca, Fe, K, Mg, Mn, Na, P, S, Si and Ti
Trace elements	As, Ba, Be, Ce, Cd, Co, Cu, La, Mo, Nd, Ni, Pb, Sr, V, Y, Zn and Zr

data is restricted to specific heavy minerals that possess a unique geochemical signature. The three main comparisons that can be constructed are Zr to zircon, Cr to chrome-spinel and Ti to rutile, anatase, brookite and titanite (ilmenite, another major Ti bearing mineral is excluded as opaque heavy minerals could not be identified) as shown in Fig. 4. Direct Cr, Ti and Zr comparisons for all samples can be found in supplementary data.

A two-tailed non-parametric test, the Mann-Whitney *U* test (Wang and Yue, 2002), was used to determine whether there was any statistical difference between the mineralogical and geochemical data. In this test, the sample populations were assigned a *Z*-score based on the normalised data. If the magnitude of this score is greater than the *Z*-critical (1.96) then there is a 95% probability that the two populations (i.e. chemistry and mineralogy) are statistically different from one another. The calculated *Z*-scores were Ti = −0.96, Cr = 3.48 and Zr = 4.43 (Fig. 4a–c). However, these values are somewhat misleading due to the provenance-specific geochemistry associated with each sample group. Therefore individual *Z*-scores were calculated for each of four sample groups in each element–mineral comparison (Table 4). Overall, most of the individual *Z*-scores indicated good agreement between the two datasets. However, the *Z*-scores for Zr (Miocene and Modern sand), Cr (Miocene) and Ti (Hili Formation) indicated that the chemical and mineralogical datasets were significantly different.

The poor *Z*-scores for Zr (Miocene: 3.52 and Dune sands: 2.68) are not necessarily reflected in Fig. 4a; the Miocene samples appear to have a greater degree of scatter whilst the Dune sands appear to plot along the 1:1 line. The sample populations associated with the *Z*-scores for Cr (Miocene: 6.01) and Ti (Hili: 3.02) appear to be discrete but biased towards the x-axis (ICP-AES) (Fig. 4b and c). The *Z*-scores for Cr (Ghayathi: −1.90) and Ti (Ghayathi: 0.82) are both below the *Z*-critical (1.96) yet plot as discrete populations which appear biased towards the Y-axis (Mineral counts) (Fig. 4b and c).

The normalised geochemical and mineralogical data were also plotted on ternary diagrams using two groups of elements that can be diagnostic of provenance: Zr, Cr, Ti and Ca, Fe, Mg. Ternary plots associated with the more resistant heavy minerals (Fig. 5a and b) were used to compare Zr, Cr and Ti with their associated minerals, i.e. zircon, Cr-spinel and transparent Ti minerals (anatase, brookite, rutile and titanite). In these plots the general population trends between the geochemical and mineralogical data are similar. Thus, the Miocene sediments are comparatively enriched in Zr and Ti, the Ghayathi and Hili formations contain more Cr than the Miocene sediments and the modern dune sands appear to cluster between the other three groups. The obvious difference between the two plots is the degree of scatter. In the geochemical plot (Fig. 5a) the populations are discrete and well defined whereas in Fig. 5b the groups are less well constrained. In contrast, the geochemistry data associated with the less resistant heavy minerals (Fig. 5c) are not as distinctive as their more resistant counterparts, which makes a direct comparison with the mineralogy difficult. Whilst the occurrence of some minerals can indicate particular source rocks (e.g. orthopyroxene is often derived from pyroxenites, peridotites and dunites, whereas the presence of clinopyroxene can indicate mafic igneous rocks) it is more difficult to associate differences in the geochemistry of the HMCs with specific rock types. However, it is still possible to infer particular geological terrains from the HMC

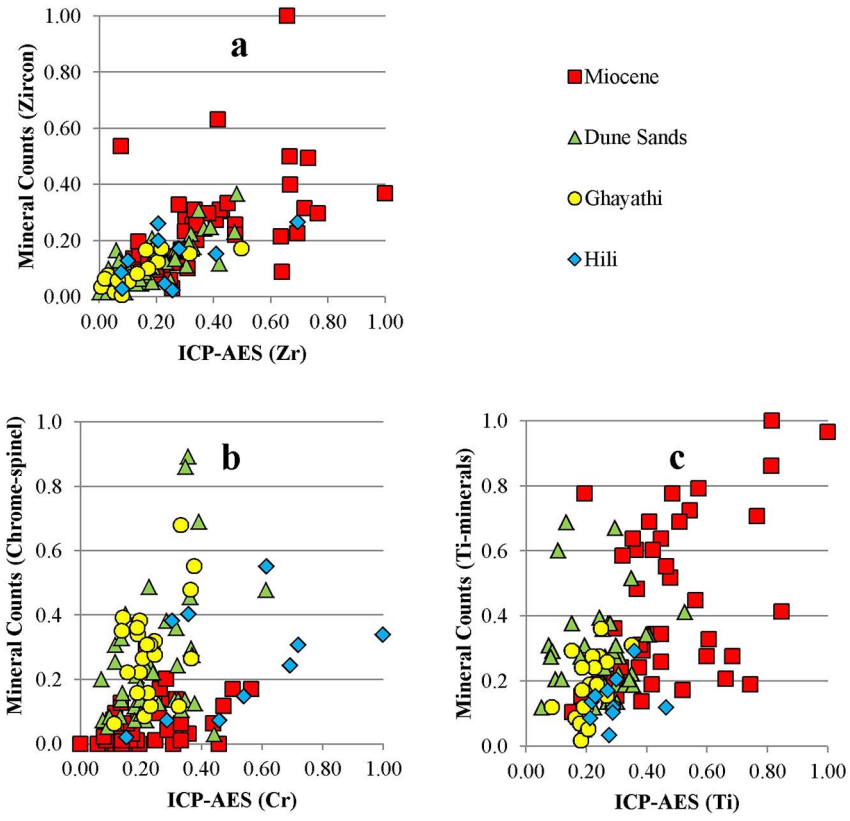

Fig. 4. Comparison of normalised mineral counts and element concentrations from UAE HMC. a, Zr:zircon. b, Cr:chrome-spinel. c, Ti:anatase, brookite, rutile, titanite.

Table 4
Non-parametric *Z*-scores for individual formations, *Z*-critical = 1.96.

Associated figure	Element	*Z*-score			
		Miocene	Hili	Ghayathi	Modern sand
3A	Zr	3.52	1.66	1.65	2.68
3B	Cr	6.01	1.97	−1.9	0.13
3C	Ti	1.07	3.02	0.82	−1.77

geochemistry.

The Hili Formation sediments are more ferromagnesian (Fig. 5c) and their mineralogy appear to be more dominated by amphibole and orthopyroxene (Fig. 5d). Most of the Miocene sediments trend towards a ferro-calcic signature (Fig. 4c); this is also reflected in their mineralogy, which is dominated by calc-amphibole and clinopyroxene (Fig. 5d).

The Ghayathi Fm geochemistry is distinctive and discrete, with consistent ratios of Mg, Ca and Fe (Fig. 5c); the associated mineralogy appears to be biased towards clinopyroxene, with subordinate calc-amphibole (Fig. 5d). Most of the modern dune sands plot within the other sediment populations, with the exception of a small but discrete population of dune sands with an enriched Ca/Mg signature that is relatively depleted in Fe (Fig. 5c). This separate group of modern dune sands is not reflected in the associated mineralogy (Fig. 5d).

5. Discussion

Several factors are likely to contribute to potential differences between the mineralogical and geochemical methods. One is the shape and volume of the minerals, which is not taken into account during typical mineral counting. Thus a small, slender, prismatic zircon crystal (~49 mm^3) would be counted the same as a larger, equant, well-rounded crystal (~1020 mm^3) but the difference in volume (mass) would affect the related Zr concentration determined by ICP-AES. In this example there is a 95% difference in volume between a slender prismatic crystal and a larger spherical grain. This phenomenon has previously been noted by Ratcliffe et al. (2007).

Differences in crystal volume can also result from the partial dissolution of specific minerals. This effect is directly related to mineral stability, weathering and diagenesis (Andò et al., 2012) and is commonly observed in less resistant minerals such as pyroxenes and amphiboles. Selective dissolution in these minerals is typically observed as 'hacksaw'-terminated crystals (Fig. 6a–c). It is difficult to assess its impact on the related geochemistry. In this study, most of the sediments are still fairly immature due to the UAE's arid environment and there is little evidence to suggest that there has been a large degree of selective dissolution. Samples with evidence of 'hacksaw' dissolution were restricted to areas in close proximity to the Arabian Gulf.

Another difference that could influence a comparison between mineralogy and geochemistry is the fact that some minerals are excluded from the mineral counts; these include opaque minerals, authigenic minerals and carbonates such as the detrital dolomite shown in Fig. 6d. This dolomitic component is described further by Lacinska et al. (2014) and also accounts for the discrete population (enriched in Ca/Mg) of dune sands described in Fig. 5c. These minerals are included in the HMC geochemistry data and therefore care must be taken when interpreting differences between the datasets.

A final difference between the two methods is related to the stoichiometry of some minerals, which can differ depending on their mode of formation (Aqrawi and Evans, 1994 and Al-Juboury et al., 2012). This particularly applies to chrome-spinel, which would affect the Cr concentration determined (Thayer, 1956) and thus the Chrome:Cr-spinel ratio. In addition, the colour and optical-transparency of Cr-spinels can potentially bias results. Cr-spinels can be identified optically as reddish-brown, dusky brown or dusky red to opaque (optically isotropic) (Thayer, 1956 and Baumgartner, 1985), the redness of Cr-spinel has been attributed to its relative chrome content (Thayer, 1956). Whilst the variations of colour and relative transparency can be accounted for optically, a suite of opaque (optically-isotropic) Cr-spinels

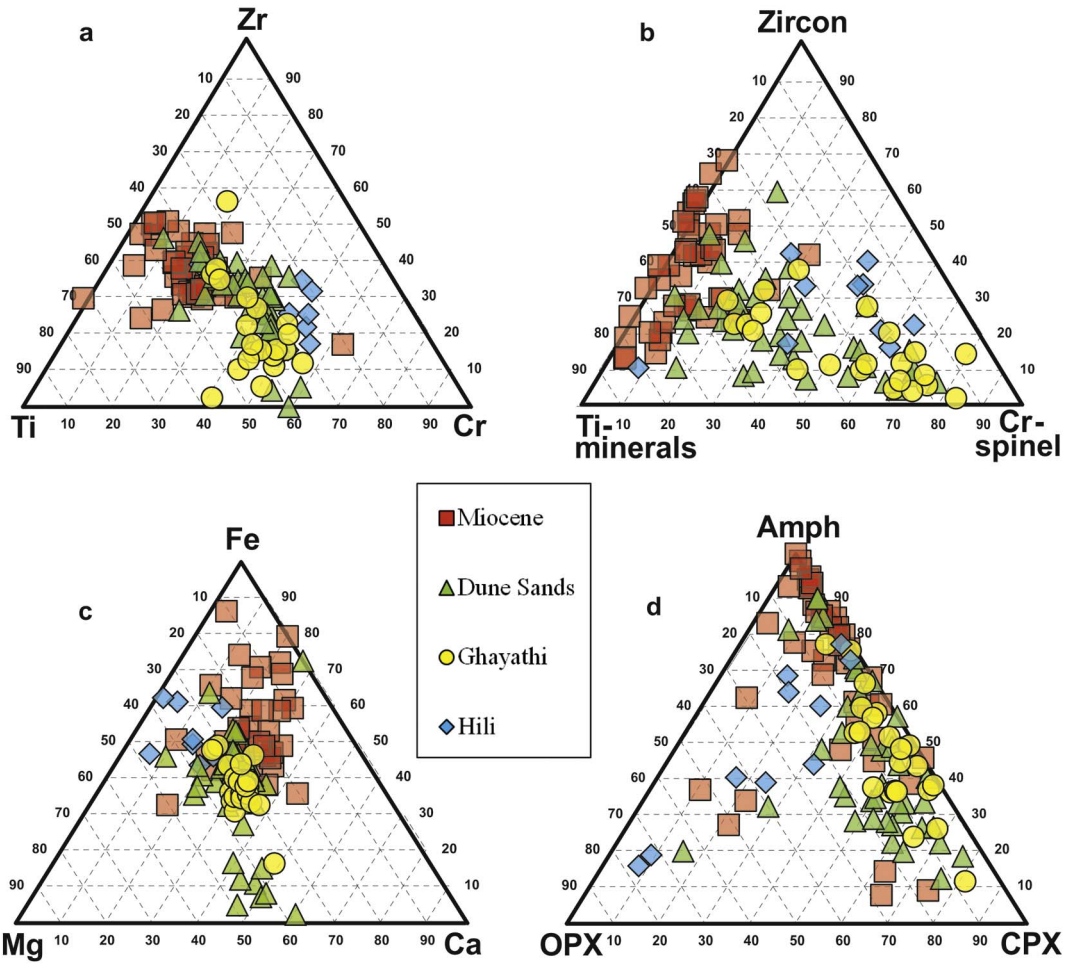

Fig. 5. a, Ternary plot of Zr, Ti and Cr. b, Ternary plot of resistant minerals (zircon, Cr-spinel and Ti-minerals [anatase, brookite, rutile, titanite]). c, Ternary plot of Fe, Mg and Ca. d, Ternary plot of less resistant heavy minerals (Cpx = clinopyroxene, Opx = orthopyroxene and Amph = amphibole).

could not and would therefore be excluded from the mineral count. And as previously mentioned (Fig. 3), a minor chemical component of a heavy mineral (e.g. Ti in Augite) may preferentially increase the overall Ti signature of the sample if a high concentration of the mineral exists.

These potential biases can assist the interpretation of data from the two techniques. For example, the greater spread of Zr concentrations in the Miocene sediments (Fig. 4a) could infer a difference in zircon grain morphology. The Cr relationship in Fig. 4b suggests that the Cr content

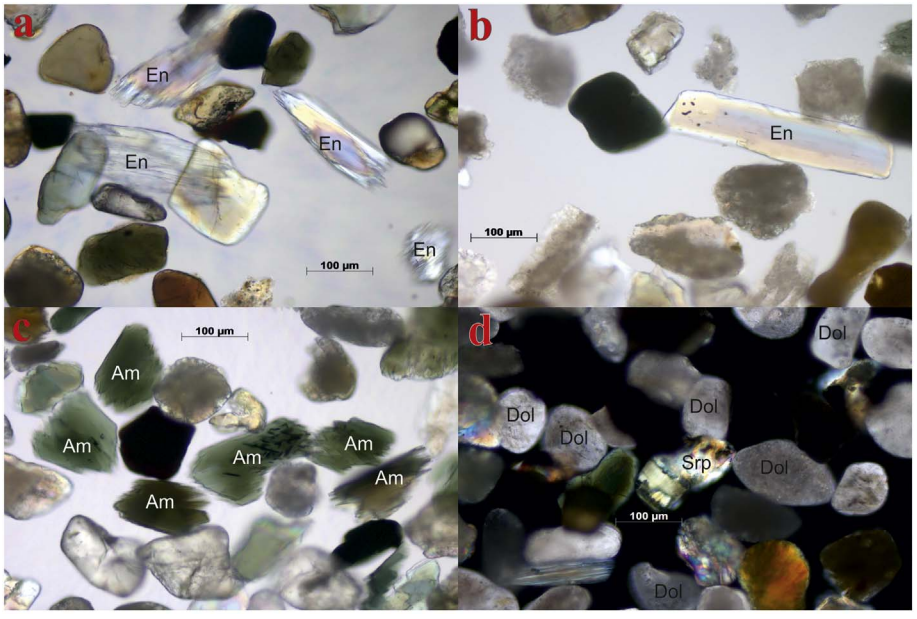

Fig. 6. Photomicrographs (plain-polarised: light-PPL, crossed-polars: XPL) showing: a, PPL photomicrograph showing selective dissolution of enstatite (En), [orthopyroxene] with hacksaw-terminated crystals; b, PPL photomicrograph showing prismatic elongate enstatite (En) crystal with no sign of selective dissolution; c, PPL photomicrograph showing hacksaw-terminated crystals of amphibole (Am) and d, XPL photomicrograph showing detrital dolomite (Dol) and serpentinite (Srp).

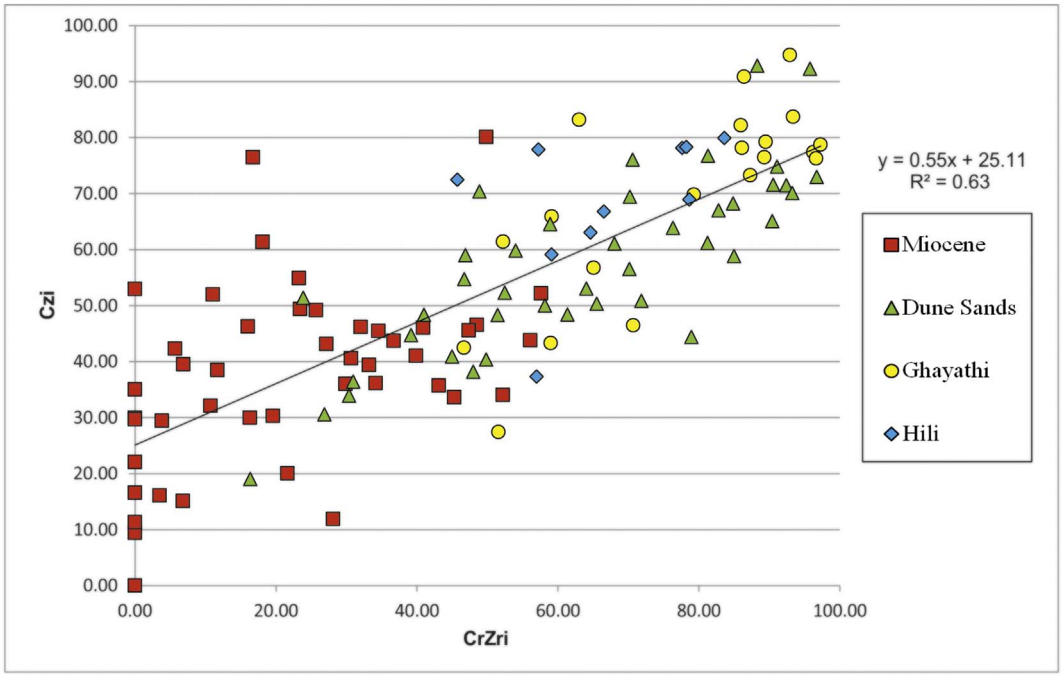

Fig. 7. Comparison of chrome-spinel:zircon index (CZi) and chromium:zirconium index (CrZri).

of the Ghayathi Formation spinels is generally lower than those associated with either the Miocene sediments or the Hili Formation. This does not, however, preclude the possibility that some Cr-spinels may have been missed during the mineral counting. The Ti comparison (Fig. 4c) appears to be the most scattered but this cannot be associated with any single factor such as grain volume, the inclusion of Ti bearing opaque minerals or variable stoichiometries, as these could all contribute to the overall deviation of data from an exact correlation.

As previously mentioned, a heavy mineral index can be used to aid the determination of sediment provenance. In this case study, the chrome-spinel:zircon index (CZi) and its corresponding geochemical index (CrZri) are the most appropriate. A direct comparison of both indices (Fig. 7) shows a positive correlation with an R^2 is of 0.63. The Mann Whitney *U* test was used to further demonstrate that the two datasets are comparable within a 95% confidence limit. This test produced a *Z*-score of 0.32, well below the *Z*-critical value of 1.96, showing that there is no statistical difference between the CZi and CrZri indices. Once again the Miocene sediments display the greatest degree of scatter, which is attributed to the disparity between the different volumes of zircons.

Indices based on mineralogical and geochemical data for each sediment type were calculated (100 × Cr / [Cr + Zr])and subdivided into three categories, low (< 33), medium (33–66) and high (> 66) – a high index is indicative of a Cr-rich, Zr-poor signature. Fig. 8a (CZi) and Fig. 8b (CrZri) display these categories with their associated locations within the UAE. The mineralogical and geochemical maps indicate similar trends, with higher CZi and CrZri indices for the Ghayathi and Hili formations and modern dune sands in the east of the UAE.

6. Conclusion

This study demonstrates the validity of a novel geochemical approach to the heavy mineral provenancing of sediments. A procedure specifically tailored to the analysis of heavy mineral concentrates by ICP-AES was developed and applied to desert sands from the United Arab Emirates. Some of the many variables associated with either analytical method were considered including grain size, mineral dissolution, the occurrence of opaque or non-detrital heavy minerals and an assumed mineral stoichiometry. In spite of this complexity, an index derived from the geochemistry of heavy mineral concentrates showed remarkably good agreement an index based purely on the optical identification of these minerals. Further interpretation and manipulation of this data is will be presented in a separate paper (Farrant et al., 2017).

The advantages of this geochemical approach include:

- Faster analysis time for large numbers of samples. This method represents a ten-fold increase in productivity compared to analysis by optical microscopy without compromising the final interpretation.
- The quantification of REE. Whilst not used in this particular case study, REE data can still be useful for particular studies.
- Geochemistry of the HMC does not discriminate between transparent and opaque heavy minerals. In particular chrome-spinel, which can be particularly difficult to identify optically.

Optical identification of HMC is still required for definitive identification of heavy minerals which lack a unique geochemical signature and for the observation of physical and chemical surface alteration. Although this geochemical method may not eliminate the need for the identification of heavy minerals by optical microscopy entirely, it can be employed as a powerful screening tool to facilitate larger scale provenance studies used in applications such as mineral reconnaissance and petroleum exploration.

Author contributions

I. Mounteney and A. Burton wrote the main manuscript text and performed all of the analytical test-work. A. R. Farrant, collected samples for analysis and reviewed the manuscript. M. J Watts, S. J. Kemp and J. M. Cook all reviewed the manuscript.

Competing financial statement

The authors declare no competing financial interests.

Acknowledgements

This paper is dedicated to the late Dr. Robert O'B Knox an expert in

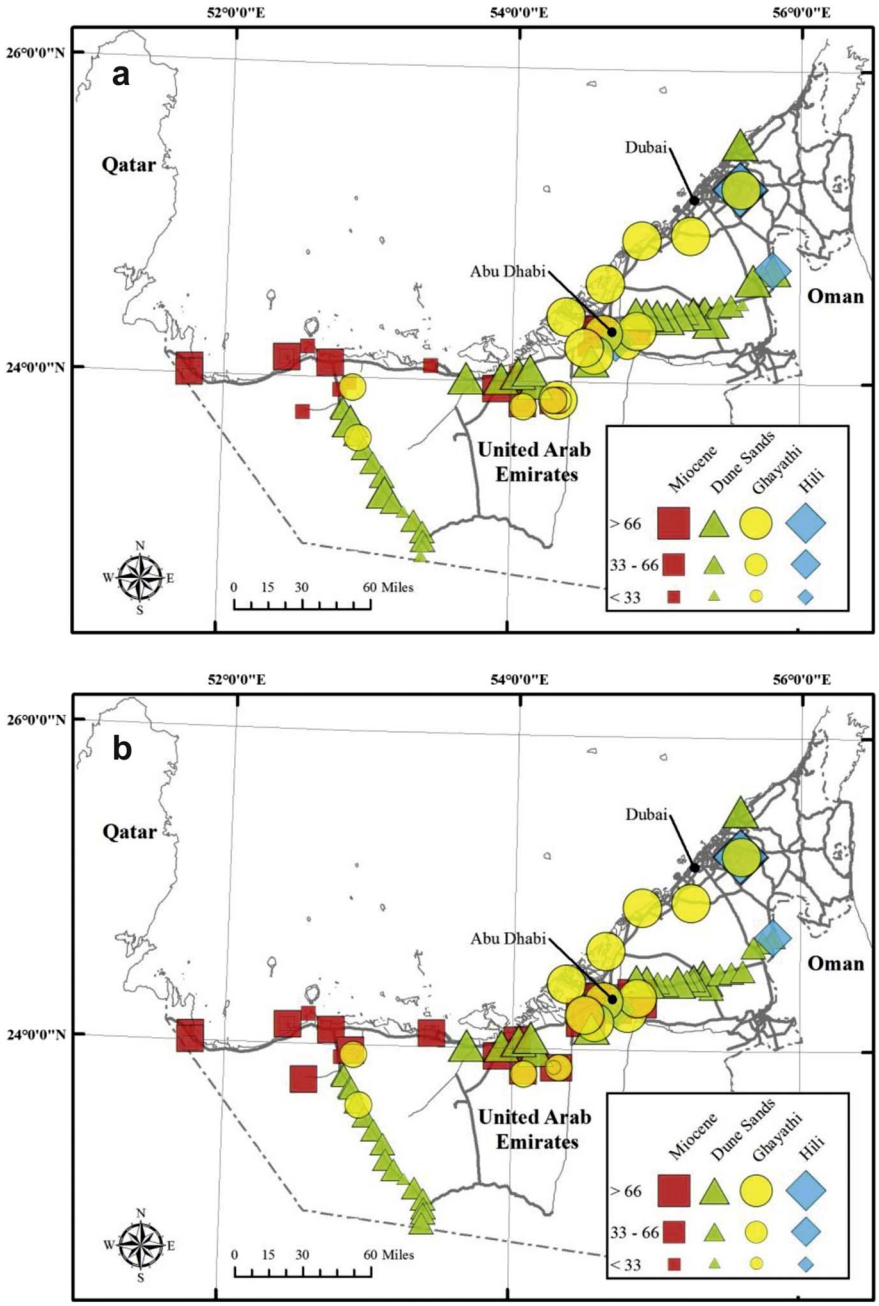

Fig. 8. a, Map of the UAE showing chrome-spinel:zircon indices (CZi) ranging from high (> 66), medium (33–66) and low (< 33), b, Map of UAE showing chromium:zirconium indices (CrZri) ranging from high (> 66), medium (33–66) and low (< 33). Map created using ArcGIS, [version 10.1], (http://desktop.arcgis.com/en/arcmap).

the identification of heavy minerals through optical microscopy and their application to sediment provenance studies. Tom Bide assisted with the collection of samples. This paper is published with the approval of the Executive Director, British Geological Survey (NERC). I would also like to thank the reviewers of this work, who helped to improve the final manuscript: Sergio Andò and anonymous.

Appendix A. Supplementary data

Science impact statement

1. Analysis of heavy minerals by ICP-AES can determine key elements associated with specific heavy minerals.
2. Capable of processing large numbers of samples rapidly as a screening technique.
3. Used in defining heavy mineral signatures in key sediments associated with conventional and unconventional energy, mineral reconnaissance and paleogeographic reconstruction.

Supporting image: Fig. 5. Supplementary data associated with this article can be found in the online version, doihttp://dx.doi.org/10.1016/j.gexplo.2017.10.007.

References

Al-Juboury, A.I., Ghazal, M.M., McCann, T., 2012. Detrital chromian spinels from Miocene and Holocene sediments of northern Iraq: provenance implications. J GEOsci 289–300.

Andò, S., Garzanti, E., Padoan, M., Limonta, M., 2012. Corrosion of heavy minerals during weathering and diagenesis: a catalogue for optical analysis. Sediment. Geol. 280, 165–178.

Aqrawi, A.A.M., Evans, G., 1994. Sedimentation in the lakes and marshes (Ahwar) of the Tigris-Euphrates Delta, southern Mesopotamia. Sedimentology 41, 155–776.

Arslan, M., Aslan, Z., 2006. Mineralogy, petrography and whole-rock geochemistry of the Tertiary granitic intrusions in the Eastern Pontides, Turkey. J. Asian Earth Sci. 27, 177–193.

Averill, S.A., 2001. The application of heavy indicator mineralogy in mineral exploration

with emphasis on base metal indicators in glaciated metamorphic and plutonic terrains. Geol. Soc. 185, 69–81.
Baumgartner, P.O., 1985. Jurassic Sedimentary Evolution and Nape Emplacement in the Argolis Peninsula (Peloponnesus, Greece). Birkhäuser (ISBN-13:978-3-0348-9994-9).
Crouvi, O., Amit, R., Enzel, Y., Gillespie, A.R., 2010. Active sand seas and the formation of desert loess. Quat. Sci. Rev. 29 (17–18), 2087–2098.
Edgell, H.S., 2006. Arabian Deserts: Nature, Origin and Evolution. Springer Netherlands, 978-1-4020-3970-6pp. 592.
Evans, G.K.A., Carter, R.A., 2002. Quaternary development of the United Arab Emirates Coast: new evidence from Marawah Island, Abu Dhabi. GeoArabia 7 (3), 441–458.
Fandrich, R. Gu, Burrows, Y.D., Moeller, K., 2007. Modern SEM-based mineral liberation analysis. Int. J. Miner. Process. 84, 310–320.
Farrant, A.R., et al., 2012. The geology and geophysics of the United Arab Emirates. In: Volume 6: Geology of the Western and Central United Arab Emirates. British Geological Survey (NERC)978-085272743-0, .
Farrant, A.R., et al., 2017. Gone with the wind: dune provenance in the northern Rub' al-Khali, United Arab Emirates, Arabia. J. Geol. Soc (in press).
Galehouse, J.S., 1971. Point counting. In: Carver, R.E. (Ed.), Procedures in Sedimentary Petrology, pp. 385–407.
Garzanti, E.A.S., Vezzoli, G., Dell'era, D., 2003. From rifted margins to foreland basins: investigating provenance and sediment dispersal across desert Arabia (Oman, UAE). J. Sediment. Res. 73 (4), 572–588.
Garzanti, E., Doglioni, C., Vezzoli, G., Andò, S., 2007. Orogenic belts and Orogenic sediment provenance. J Geol. 115 (3), 315–334.
Garzanti, E., et al., 2013. Provenance and recycling of Arabian desert sand. Earth Sci. Rev. 120, 1–19.
Glennie, K.W., Singhvi, A.K., 2002. Event stratigraphy, paleoenvironment and chronology of SE Arabian deserts. Quat. Sci. Rev. 21 (7), 853–869.
Hounslow, M.W., Morton, A.C., 2004. Evaluation of sediment provenance using magnetic mineral inclusions in clastic silicates: comparison with heavy mineral analysis. Sediment. Geol. 171, 13–36.
Joy, E.J.M., et al., 2015. Soil type influences crop mineral composition in Malawi. Sci. Total Environ. 505, 587–595.
Kumar, A., Abdullah, M.M., 2011. An overview of origin, morphology and distribution of desert forms, sabkhas and playas of the Rub' al Khali desert of the southern Arabian Peninsula. Earth Sci. India 4 (III), 105–135.
Kumar-Jain, Y., Bhandare, S.K., 2011. Min max normalization based data perturbation method for privacy protection. Int. J Compute. Commun. Technol. 2 (8), 45–50.
Lacinska, A.M., Styles, M.T., Farrant, A.R., 2014. Near-surface diagenesis of ophiolite-derived conglomerates of the Barzaman Formation, United Arab Emirates: a natural analogue for permanent CO_2 sequestration via mineral carbonation of ultramafic rocks. Geol. Soc. Lond., Spec. Publ. 392 (1), 343–360.
Lapworth, D.J., et al., 2012. Geochemical mapping using stream sediments in west-central Nigeria: implications for environmental studies and mineral exploration in West Africa. Appl. Geochem. 27 (6), 1035–1052.
Luepke, G., 1980. Opaque minerals as aids in distinguishing between source and sorting effects on beach-sand mineralogy in southwestern Oregon. J. Sediment. Petrol. 50, 489–496.
Miles, D.M., Cook, J.M., 2007. Geological applications of plasma spectrometry. In: Hill, S.J. (Ed.), Inductively Coupled Plasma Spectrometry and its Applications, 2nd edition. Blackwell Publishing Ltd, pp. 277–337.
Morton, A.C., Berge, C., 1995. Heavy mineral suites in the Statfjord and Nansen Formations of the Brent Field, North Sea; a new tool for reservoir subdivision and correlation. Pet. Geosci. 1, 355–364.
Morton, A.C., Hallsworth, C.R., 1993. Identifying provenance-specific features of detrital heavy mineral assemblages in sandstones. Sediment. Geol. 90, 241–256.
Morton, A.C., Hallsworth, C.R., 1999. Processes controlling the composition of heavy mineral assemblages in sandstones. Sediment. Geol. 124, 3–29.
Pearce, T.J., Martin, J.H., Cooper, D., Wray, D.S., 2010. Chemostratigraphy of Upper Carboniferous (Pennsylvanian) sequences from the southern North Sea (United Kingdom). Society for Sediment. Geol. 94, 109–127.
Pe-Piper, G., et al., 2016. Quaternary evolution of the rivers of northeast Hainan Island, China: tracking the history of avulsion from mineralogy and geochemistry of river and delta sands. Sediment. Geol. 333, 84–99.
Ratcliffe, K.T., Morto, A.C., Ritcey, D.H., Evenchick, C.A., 2007. Whole-rock geochemistry and heavy mineral analysis as petroleum exploration tools in the Bowser and Sustut basins, British Columbia, Canada. Bull. Can. Petrol. Geol. 55 (4), 320–336.
Sukhorukov, V.P., 2007. Composition and conditions of formation of andalusite-kyanite-sillimanite pegmatoid segregations in metamorphic rocks of the Tsel block (Mongolian Altay). Russ. Geol. Geophys. 48, 478–482.
Thayer, T.P., 1956. Mineralogy and geology of chromium. Chromium. Chemistry of chromium and its compounds. Amer. Chem. Soc. Monograph 1132, 14–52.
Wallace, M.L., Jowitt, S.M., Saleem, A., 2015. Geochemistry and petrogenesis of mafic–ultramafic suites of the Irindina Province, Northern Territory, Australia: implications for the Neoproterozoic to Devonian evolution of central Australia. Lithos 234–235, 61–78.
Wang, C.Y., Yue, S., 2002. The influence of serial correlation on the Mann–Whitney test for detecting a shift in median. Adv. Water Resour. 25, 325–333.
Watts, M.J., Chenery, S.R., 2010. Report on results of overseas analysis: unprocessed data. In: Nigerian Geochemical Mapping Technical Assistance Project. British Geological Survey Commissioned Report (CR/10/020 60 pp).
Watts, M.J., Button, M., Brewer, T.S., Jenkin, G.R.T., Harrington, C.F., 2008. Quantitative arsenic speciation in two species of earthworms from a former mine site. J. Environ. Monit. 10, 753–759.
Weltje, G.J., Eynatten, H.V., 2004. Quantitative provenance analysis of sediments: review and outlook. Sediment. Geol. 171 (1–4), 1–11.
Worobiec, A., Stefaniak, A.E., Potgieter-Vermaak, S., Sawlowicz, Z., Spolnik, Z., Van Grieken, R., 2007. Characterisation of concentrates of heavy mineral sands by micro-Raman spectrometry and CC-SEM/EDX with HCA. Appl. Geochem. 22 (9), 2078–2085.